Phytoglycogen Nanoparticles: Nature-Derived Superlubricants

Journal:	*ACS Nano*
Manuscript ID	nn-2021-01755k.R3
Manuscript Type:	Article
Date Submitted by the Author:	04-May-2021
Complete List of Authors:	Adibnia, Vahid; University of Toronto Ma, Yingshan; University of Toronto Halimi, Ilias; University of Toronto Walker, Gilbert; University of Toronto, Department of Chemistry; Banquy, Xavier; Universite de Montreal, Faculty of Pharmacy Kumacheva, Eugenia; University of Toronto, Department of Chemistry

Phytoglycogen Nanoparticles: Nature-Derived Superlubricants

Vahid Adibnia [a,b], Yingshan Ma [a], Ilias Halimi[a], Gilbert C. Walker[a], Xavier Banquy [b]*, and Eugenia Kumacheva [a,c,d]*.

a Department of Chemistry, University of Toronto, Toronto, Ontario, Canada, M5S 3H6.

[b] Faculty of Pharmacy, Université de Montréal, Montreal, Quebec, Canada, H3C 3J7.

c Institute of Biomedical Engineering, University of Toronto, Toronto, Canada, M5S 3G9.

[d] Department of Chemical Engineering and Applied Chemistry, University of Toronto, Toronto, Canada, M5S 3E5.

*Corresponding Authors

eugenia.kumacheva@utoronto.ca;

xavier.banquy@umontreal.ca;

Supporting Information available

ABSTRACT: Phytoglycogen nanoparticles (PhG NPs), a single-molecule highly branched polysaccharide, exhibit excellent water retention, due to the abundance of close-packed hydroxyl groups forming hydrogen bonds with water. Here we report lubrication properties of close-packed adsorbed monolayers PhG NPs acting as boundary lubricants. Using direct surface force measurements, we show that the hydrated nature of the NP layer results in its striking lubrication performance, with two distinct confinement-controlled friction coefficients. In the weak-to-moderate confinement regime, when the NP layer is compressed down to 8 % of its original thickness under a normal pressure of up to 2.4 MPa, the NPs lubricate the surface with a friction coefficient of 10^{-3}. In the strong-confinement regime, with 6.5% of the original layer thickness under a normal pressure of up to 8.1 MPa, the friction coefficient was 10^{-2}. Analysis of the water content and energy dissipation in the confined NP film reveals that the lubrication is governed by synergistic contributions of unbound and bound water molecules, with the former contributing to lubrication properties in the weak-to-moderate confinement regime and the latter being responsible for the lubrication in the strong-confinement regime. These results unravel mechanistic insights that are essential for the design of lubricating systems based on strongly hydrated NPs.

Keywords: biolubrication; nanoparticles; phytoglycogen; green chemistry; branched polymers

Moving parts in mechanical, biological, and biomedical systems require constant lubrication. Biolubrication is particularly challenging, as the lubricant choice is limited by the requirements for its biocompatibility and low cytotoxicity. Fortunately, nature serves a source of inspiration for designing biolubrication systems. For example, healthy human synovial joints function at a friction coefficient as low as ~10^{-3}-10^{-2}.[1,2] Excellent lubrication in the joints is achieved by synergistic contributions of different macromolecular components in the synovial fluid, including hyaluronic acid, phospholipids, and proteoglycans.[3–5] Although none of these macromolecules can individually provide efficient lubrication of joints at high pressures, they form boundary layer lubricating complexes with each other at the cartilage interface, which are believed to be responsible for joint lubrication.[4]

From the molecular perspective, the primary role of lubricating macromolecules in a lubrication system is to improve the distribution and retention of water at the liquid-solid interface.[6,7] These macromolecules retain water at the solid/liquid interface in the form of sub-nanometric hydration layers,[8,9] which sustain normal pressures of up to several tens of MPa.[6] When the surfaces slide past each other, even on dissimilar surfaces,[10] these layers significantly reduce friction *via* the mechanism that originates from energy dissipation in the hydration shells around hydrophilic moieties.[11] In the absence of hydration layers, sliding of molecules past each other generates a strong friction force. The hydration lubrication mechanism has been used for the design of synthetic polymeric lubricants, *e.g.*, polyelectrolytes,[12,13] zwitterionic polymers,[14,15] and polysaccharides,[16,17] all exhibiting high water retention when adsorbed or grafted to different surfaces, and resulting in friction coefficients below 10^{-2}.

Polymer conformation at the solid-liquid interface depends on density of the polymer surface-attached layers, entanglement of polymer molecules, and water retention properties of the polymer film, all of which play a key role in its lubrication performance.[1] Lubrication properties of end-tethered polymer molecules in a brush-like configuration, bottlebrushes, and branched and crosslinked polymers have been extensively studied.[1] Over the past few years, however, polymeric nanoparticle- or microparticle-based lubricants have attracted special attention, with a focus on their applications in synovial joint lubrication.[18–20] One of the advantages of such systems is that, in addition to lubrication, particles enable the encapsulation and release of active therapeutic agents.[21] It has been hypothesized that soft NPs may lubricate by a rolling mechanism, similar the lubrication mechanism of hard NPs, *e.g.*, carbon microspheres.[22] Yet, considering the nature of hydrated lubricating polymeric NPs with elastic modulus on the order of several kPa,[23,24] NP rolling on the surface is unlikely, especially, when they are confined under the pressure of a few MPa. Notably, despite the lack of comprehensive mechanistic studies on lubrication by polymeric

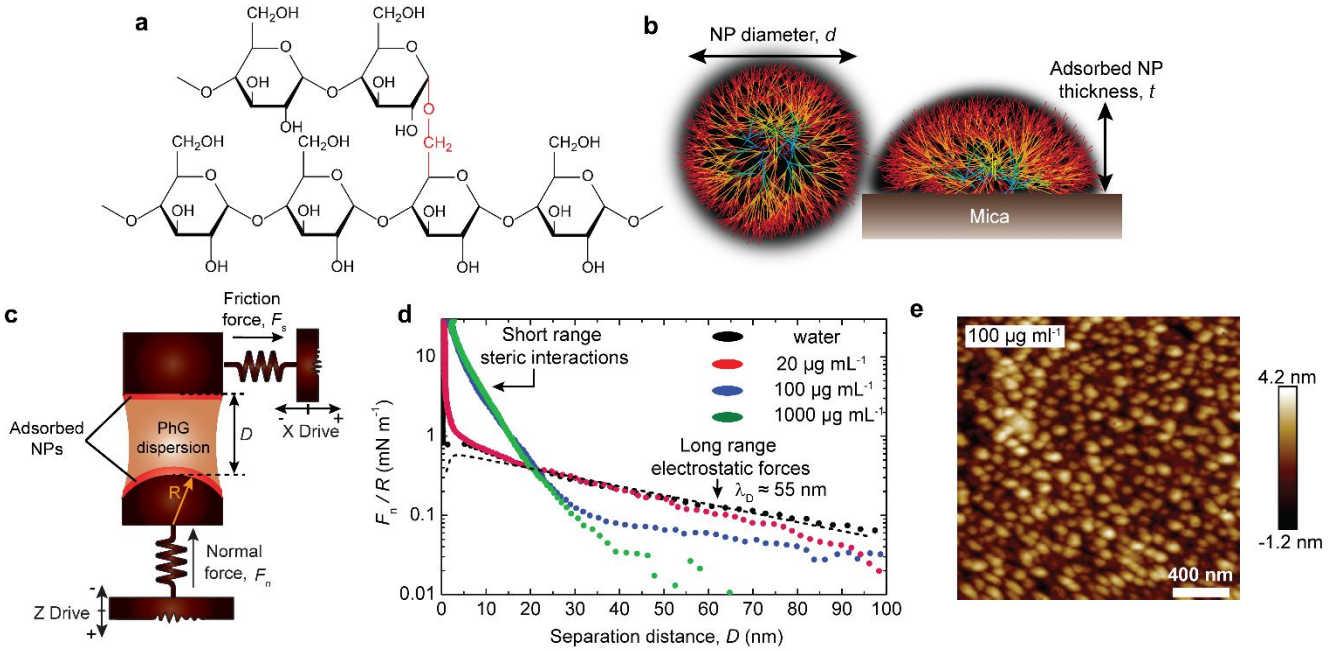

Figure 1. (a) Chemical structure of highly branched PhG NPs made of glucose monomers. The red color highlights the position of branching in the chain. (b) Schematic representation of the globular NPs in aqueous dispersions (left) and physically adsorbed on mica (right). (c) Schematic representation of the SFA setup for normal and friction force measurements. Dispersions of PhG NPs with different concentrations were injected between mica surfaces, forming a layer of adsorbed NPs on each surface. (d) Compression force profiles for PhG dispersions between mica surfaces at 0, 20, 100 and 1000 μg ml^{-1} PhG concentrations. The force profiles did not change at concentrations higher than 100 μg ml^{-1}. The long-range part of the force profile is attributed to the electrostatic repulsive interactions between mica surfaces across water, with a decay length, $\lambda_D \approx$ 55 nm, evaluated by $F/R \sim \exp(-\lambda_D{}^{-1} D)$, corresponding to the Debye length of a 3×10^{-5} M monovalent electrolyte solution. The dashed line is a fit to the Derjaguin-Landau-Vervey-Overbeek theory based on analytical equations described in Section S3 (Supporting Information). (e) An AFM image of PhG NPs adsorbed on a mica surface from a 100 μg ml^{-1} PhG dispersion. The adsorbed film was dried for imaging. AFM images of PhG NPs adsorbed on a mica surface from dispersions with NP concentration from 0 to 1000 μg ml^{-1} are shown in Figure S3 (Supporting Information).

NPs, the highly hydrated nature of polymers in these NPs would be a plausible explanation for their lubrication performance.

In the present study, we report outstanding boundary lubrication performance of highly branched polysaccharide PhG NPs. These NPs are produced by some plants as glucose storage units, and are most abundantly found in kernels of sweet corn.[25] During PhG polymerization and branching in the plants, the NP grows, until the polymer density in the outer region is sufficiently high, such that the enzymes catalyzing further NP growth are sterically blocked.[26] Therefore, a globular macromolecule is formed with a diameter of 30-100 nm (depending on the plant source) and narrow size distribution is formed.[27] Theoretically, 13 generations of branching are possible in these NPs.[28] The NPs exhibit excellent water retention, due to the abundance of hydroxyl groups forming hydrogen bonds with water. Attenuated total reflection infrared spectroscopy studies of PhG NPs showed that their branched architecture and high density of hydroxyl groups result in oriented and ordered structure of water within the NPs, which explains their superior water retention properties.[29] Based on the results of small-angle neutron scattering (SANS), each glucose unit is associated to 22 water molecules, equivalent to a hydration number of 7 water molecules per hydroxyl group.[27] This hydration capacity is significantly high, when compared to other mono-, di-, oligo- and poly-saccharides, such as glucose,[30] sucrose,[30,31] maltodextrin,[30] cellulose ethers,[32] and branched polyglycerols,[33] in all of which 2-4 water molecules are associated with each hydroxyl group. Using SANS analysis, the density of polymer branches in PhG NPs was found to be uniform, due to the folding back of the flexible glucose chains into the center of the NPs.[34] Rheological characterization indicates that dispersion of these NPs undergo liquid-to-gel transition at ≈ 29 wt% polymer concentration,[35] which is equivalent to the concentration of polymer in a single PhG NP.[27,34,36] Above this concentration, an increase in the osmotic pressure induces NPs dehydration and causes an increase in NP bulk modulus.[36] The physiochemical properties of PhG NPs have been recently reviewed.[26]

Using the surface force apparatus (SFA) experiments, we show excellent lubrication behavior of hydrated PhG NP layers confined between two solid surfaces. These NPs adsorbed to mica due to hydrogen bonding between NP hydroxyl groups and silanol groups on the mica surface. At intermediate pressures of up to 2.4 MPa, the NPs layers exhibit a friction coefficient of ~ 10^{-3}, whereas at higher pressures of up to 8.1 MPa, the friction coefficient does not exceed ~ 10^{-2}. These friction coefficients are in the range of 10^{-3}-10^{-2} reported for polymeric soft NP-based lubricating systems,[24,37] and are in the range of 10^{-4}-10^{-2} reported for the state-of-the-art synthetic polyelectrolyte and zwitterionic brushes.[12–15,38] We show correlation between the lubrication properties of PhG NPs and the state and amount of hydration water at different degrees of the layer compression, thereby providing insights on the lubrication mechanism of soft NP-based lubricating systems. Importantly, we achieved a striking lubrication performance by using biosourced polymeric NPs that not only fulfill the requirements for hydration lubrication, but are also cytocompatible and bioactive,[39] and have a strong potential for delivering active pharmaceutical ingredients.[40,41]

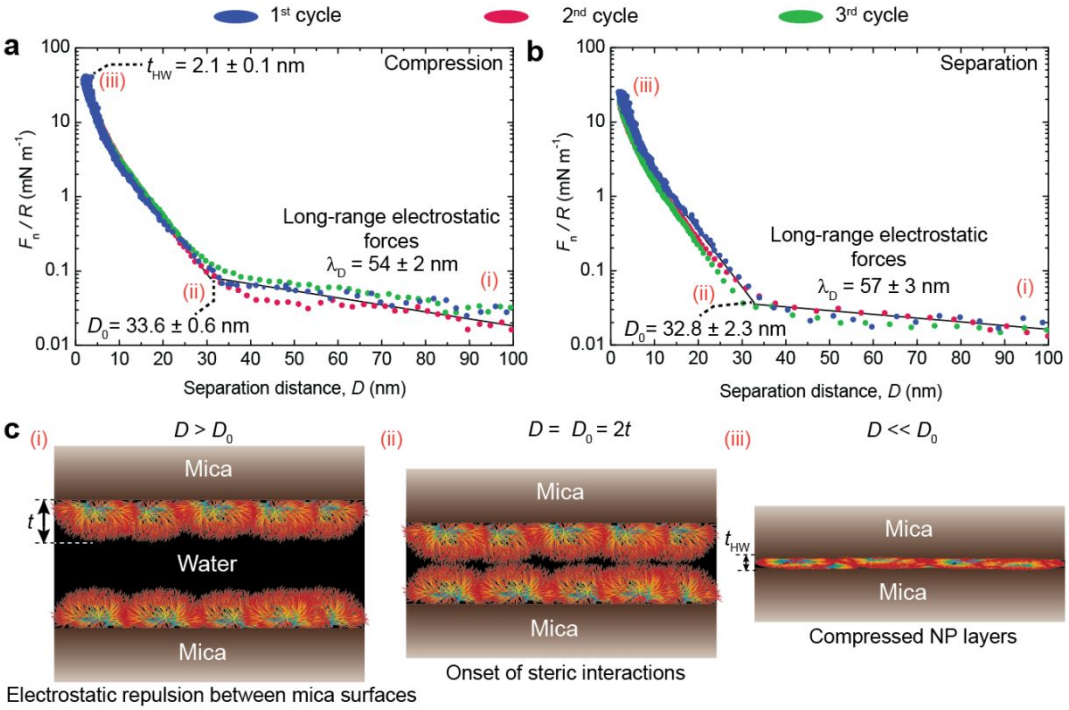

Figure 2. Interaction forces between adsorbed PhG NP films under consecutive compression-separation cycles. Compression (a) and separation (b) force profiles for mica surfaces across 100 μg ml^{-1} dispersion of PhG NPs. The compression-separation cycles were performed on the same contact area without delay between cycles. The NP films were compressed down to a hard-wall thickness $t_{HW} \approx$ 2.1 nm. The onset of steric interactions, $D_0 = 2t$, where t is the adsorbed NPs thickness on one surface. The solid lines are to guide the eyes. (c) Schematic representation of the polymer films when the surfaces are far apart (i), when they come into initial contact, $D = D_0$, (ii), and when they are compressed down to their hard-wall thickness (iii). These states were reached reversibly during compression and separation of the films in multiple cycles, suggesting sponge-like behavior of the NPs.

RESULTS AND DISCUSSION

Figure 1a shows the chemical structure of PhG NPs. The polysaccharide chains are branched every 10-12 monomer units, which corresponds to a chain length of ≈ 8.5 nm between each branching point, based on the reported 0.17 nm^3 volume of a glucose monomer in PhG.[27] Figure 1b schematically illustrates a PhG NP. The hydrodynamic radius of PhG NPs in deionized water was 33 nm, with a polydispersity index of 0.07, and ζ-potential of 0.73 ± 0.43 mV (Figure S1, Supplementary Information). On the surface of mica, based on atomic force microscopy (AFM) imaging, the adsorbed hydrated NPs spread in a pancake configuration (Figure 1b, right) with a maximum thickness of 12.5 nm.[27]

Normal forces between surfaces coated with adsorbed PhG NPs. A dispersion of PhG NPs was injected between two atomically smooth mica surfaces, as shown schematically in Figure 1c, and incubated for one hour for NP adsorption. The concentration of PhG NPs in the dispersion, C_{NP}, was varied between 0 to 1000 μg mL^{-1}. Figure 1d shows the normal force profiles, F_n (D) /R, measured upon surface approach and plotted *vs.* the distance, D, between the surfaces Here, F_n is the normal interaction force and R is the radius of the surface curvature (R = 2 cm). Each surface force profile in Figure 1c corresponds to the NP layer formed at a particular C_{NP} (Figure S2, Supporting Information shows three force profiles at each C_{NP}). The interaction forces between the negatively charged mica surfaces[42] across deionized water exhibited a strong short-range van der Waals attraction at D < 5 nm, and a long-range repulsive electrostatic interactions that exponentially decayed with D, with a decay length of $\lambda_D \approx$ 55 nm, in agreement with the previously reported force profiles measured in purified water.[14,43] With the PhG NP layer formed from the dispersion at C_{NP} = 20 μg mL^{-1}, the normal force profile between the surfaces did not significantly change compared to that in pure water. The AFM image of the surface with 20 μg mL^{-1} PhG NPs concentration (Figure S3, Supporting Information) shows that at this concentration, isolated PhG NPs are attached to the mica surface, while most of the surface remains uncovered. These individual adsorbed NPs are expected to initiate steric interactions upon compression of the film. Figure 1d shows this steric interaction of the surfaces as a weak increase in the normal force at D < 6.5 nm, when the surfaces were exposed to 20 μg mL^{-1} PhG NP dispersion. Beyond this distance, electrostatic interactions screened steric interactions. Increasing C_{NP} to 100 μg mL^{-1} led to the formation of a close-packed PhG NP layer on the mica surface (Figure 1e). Adsorption of NPs resulted in the change of short-range forces at D < 35 nm, while the exponential decay of the long-range repulsion remained invariant, compared to that in water. No further change in the force profile was observed at C_{NP} = 1000 μg mL^{-1}, as the surface was already completely covered with the NPs adsorbing from the 100 μg mL^{-1} dispersion (Figure S3, Supporting Information). This effect also indicated the absence of NP multilayers on the surfaces. We attribute a significant increase in the short-range forces at $C_{NP} \geq$ 100 μg mL^{-1} to repulsive steric interactions between the PhG NP layers adsorbed on mica surfaces.

Further studies of normal and friction forces were conducted for PhG NP layers formed on mica from the dispersion with C_{NP} = 100 μg mL^{-1}. Adsorbed NP layers on the same contact area were compressed (Figure 2a) and decompressed (Figure 2b) in three successive cycles that were conducted immediately after each other, with each cycle completed in approximately 200 s. In the compression and separation force profiles, the decay lengths of the long-range interaction forces λ_D = 54 ± 2 nm and λ_D = 57 ± 3 nm, respectively, were consistent with the decay lengths of electrostatic interaction forces observed in pure water (λ_D = 55 ± 2 nm). In all compression cycles, the steric repulsion was detected at a D_0 = 33.6 ± 0.6 nm, and consistently, disappeared at D_0 = 32.8 ± 2.3 nm upon decompression. Considering that adsorbed NPs cover both surfaces, from the onset of steric repulsion, we conclude that the thick-ness of the adsorbed PhG NP layer was $t = D_0/2$ = 16.2 ± 0.7 nm, which is close to 12.5 nm measured in AFM experiments.[27] Although the NP layers were compressed to a hard-wall thickness of 2.1 nm (the minimum distance between the surfaces achieved upon compression), and potentially, exuded most of their hydration water, the thickness t of the hydrated PhG NP layer did not change in multiple cycles. This effect suggests reversible swelling/deswelling and sponge-like behavior of the NP layer. The perfect recovery of the adsorbed NPs in multiple compression-separation cycles suggests weak and transient (or the absence of) entanglement and/or attractive intermolecular interactions between the polymer branches of the NPs, even under strong compressive forces. Highly repulsive intermolecular interactions and the absence of entanglement have been reported previously for other highly branched polymers,[44–46] In adsorbed PhG NPs layers, hydration and steric repulsive interactions between polymer branches are responsible for this behavior. Theoretical analysis predicts that repulsive intermolecular interactions of branched polymers can potentially, provide them with excellent lubrication properties.[45]

Overall, the behavior of PhG NPs in compression-separation cycles followed three regimes (Figure 2c): (i) at large separation distances, with $D > D_0$, the NP layers on the approaching surfaces were not in contact, and the resulted normal force originated from the long-range repulsive electrostatic interactions between the mica surfaces in water; (ii) At $D = D_0$, adsorbed layers came in contact, which resulted in repulsive steric interactions between the surfaces; (iii) At $D < D_0$, adsorbed NP layers were compressed and lost their hydration water (will be confirmed in this study). These three regimes were reproducible in multiple compression/decompression cycles.

Lubrication properties of adsorbed PhG NP films. Friction forces were studied for the PhG NP layers adsorbed from the dispersions with NP concentration of 100 μg ml^{-1}. A triangular oscillatory voltage applied to a piezo bimorph slider driving the bottom surface (Figure 3a, top) induced back-and-forth motion to this surface. This sliding motion generated a lateral force, F_{ll}, transmitted to the upper surface through the confined NP layer. Figure 3a, bottom shows an example of shear force traces. The shape of these races indicates that the sign of the measured lateral force alternates between negative and positive depending on the sliding direction. The amplitude of the oscillation of F_{ll} (corresponding to the friction force, F_s) exhibited an order of magnitude difference between low and high normal loads, F_n = 0.7 mN (P = 1.2 MPa, red traces) and 8 mN (P = 5 MPa, black traces), thus corresponding to the moderate and strong layer confinement, respectively. Figure 3b shows that F_s increases linearly with the normal force and exhibits two lubrication regimes, characterized by different slopes. A weak-to-moderate-confinement regime (also shown in the inset of Figure 3b at

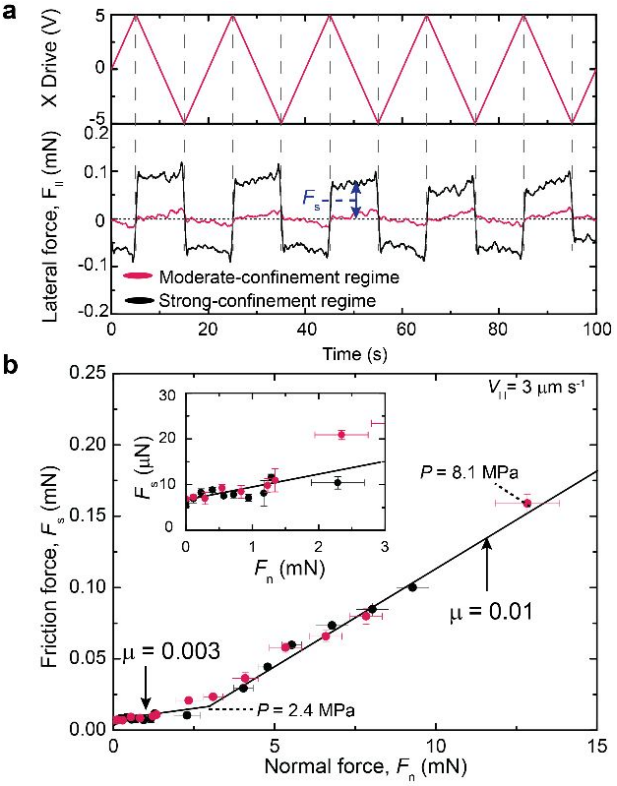

Figure 3. Lubrication properties of adsorbed PhG NP films. (a) Friction traces for mica surfaces sliding across adsorbed PhG NP films at 50 mHz (equivalent to 3 μm s^{-1}). During each shearing cycle, the oscillatory applied voltage to the friction device (shown in the top panel) induces a lateral force, F_{ll}, with an averaged amplitude equivalent to the friction force, F_s (bottom panel). Red and black traces in the bottom panel correspond to F_n of 0.7 and 8 mN, respectively. (b) Variation in friction force, F_s, *vs.* the normal force, F_n, for the confined PhG NP layers at a sliding velocity of 3 μm s^{-1}. The low-confinement regime with friction coefficient μ = 0.003 ± 0.002, persists until a normal F_n = 3.0 mN (equivalent to pressure of P = 2.4 MPa) at a separation distance D = 2.6 nm. The strong confinement regime, with μ = 0.013 ± 0.001, was tested up to a normal force of 12.8 mN (equivalent to pressure of 8.1 MPa) at a separation distance D = 2.1 nm. Inset shows the magnified region at F_n < 3.0 mN. Black and red show two independent measurements.

higher magnification) existed at F_n < 3.0 mN (equivalent to P < 2.4 MPa, separation distance of 2.6-32 nm, and degree of confinement, D/D_0, from 1.0 to 0.08). A strong confinement regime corresponded to a high normal load of 3.0 ≤ F_n ≤ 12.8 mN (equivalent to 2.4 ≤P ≤8.1 MPa, separation distance of 2.6-2.1 nm, and degree of confinement, D/D_0, from 0.08 to 0.06). The corresponding values of the friction coefficient, $\mu = F_s/F_n$, were 0.003 ± 0.002 and 0.013 ± 0.001 for these two regimes, respectively, demonstrating superlubrication performance of the adsorbed PhG NP layer, that is lubrication properties with $\mu < 10^{-2}$.[15,37] Real-time monitoring of the deformation of fringes of equal chromatic order (FECO) revealed that no damage was detected to the sliding surfaces up to 8.1 MPa pressure (Figure S4), suggesting excellent wear-resistant properties of the NP layer.

To gain insight into the lubrication mechanism by PhG NPs, we examined the correlation between the variation in the friction force and the content of water of the confined layer. The latter

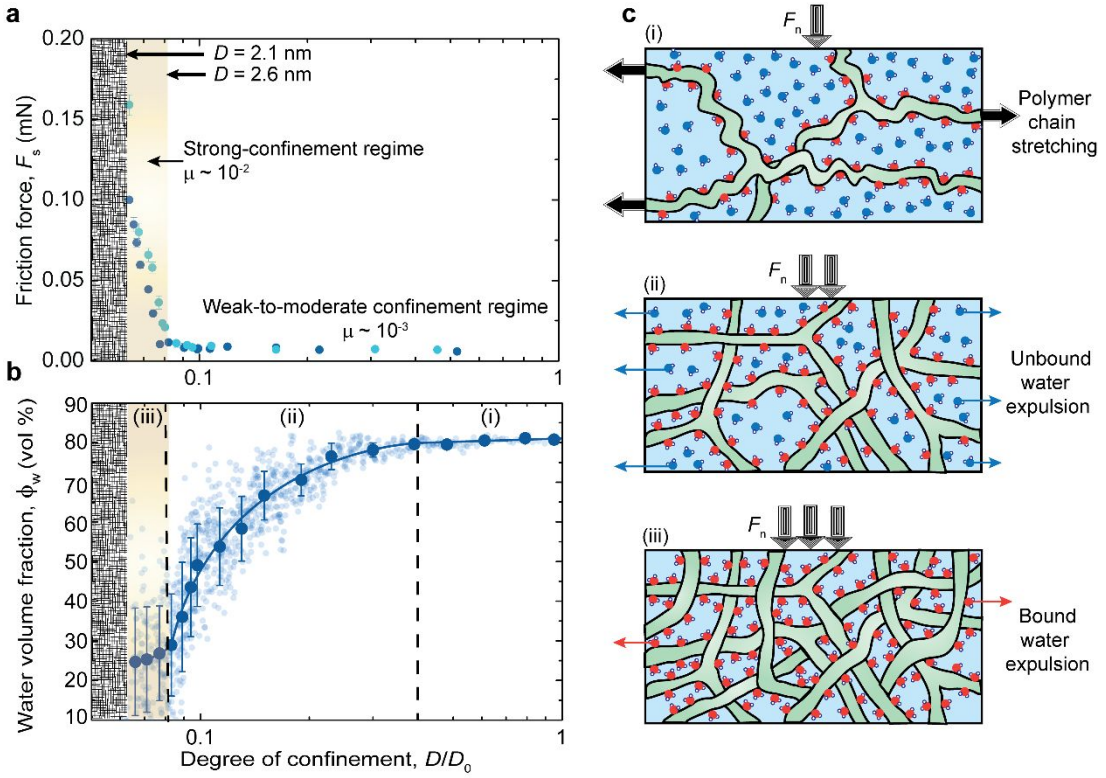

Figure 4. Compression-induced dehydration of the polymer films. (a) Variation of the friction force with distance, D, scaled with the onset of steric interactions, $D_0 \approx 32.4$ nm, when the NPs were gradually compressed under the applied normal force. In the weak-to-moderate-confinement lubrication regime, where $\mu = 0.003 \pm 0.002$, adsorbed NPs were compressed to a thickness of 2.6 nm (1.3 nm on each surface). In the strong-confinement regime (highlighted in yellow color), where $\mu = 0.013 \pm 0.001$, the NP film thickness decreased moderately to 2.1 nm. The patterned area at $D < 2.1$ nm shows the polymer films at their highest compression limit. Dark and light blue show the same two independent measurements as in Figure 3b. (b) The variation of the water volume fraction with the degree of confinement. The scattered data points are shown in light-blue color, while the averaged data points at different degrees of confinement are shown in dark-blue. Regions (i), (ii) and (iii) indicate weak-, Moderate-, and strong-confinement regimes. (c) Schematic representation of water expulsion from the NP layer at three regimes of film compression shown in panel b. Unbound and bound water molecules are shown in blue and red, respectively. Blue and red arrows illustrate unbound and bound water expulsion, respectively. The black arrow show polymer chain stretching and lateral deformation.

property was determined by *in situ* measurement of the refractive index of the confined film under compression (Figure S5, Supporting Information shows the relationship between the refractive index and polymer volume fraction). Figure 4a shows the variation of F_s with the degree of PhG NP layer confinement, defined as D/D_0, where $D_0 = 32.4 \pm 1.7$ nm is the onset of steric interactions between the films at the opposing surfaces. Figure 4b shows the corresponding variation in the water volume fraction, ϕ_w, of the confined layer. In the weak-to-moderate confinement regime, $0.08 < D/D_0 < 1.0$, the magnitude of F_s was of the order of ~10^{-2} mN, and the corresponding variation in water volume fraction exhibited two distinct behaviors. In the weak confinement regime, $0.4 < D/D_0 < 1.0$, with the thickness of the PhG NP layer decreasing from 32.4 to 13 nm, the variation in ϕ_w *vs*. compression was insignificant, that is, from 80.8 ± 0.2 to 79.6 ± 0.9 vol%. In the moderate confinement regime at $0.08 < D/D_0 < 0.40$, the decrease in ϕ_w was from 79.6 ± 0.9 to 28.9 ± 12.8 vol%. On the other hand, in the strong confinement regime at $D/D_0 < 0.08$, the value of F_s significantly increased to ~10^{-1} mN, and the corresponding layer thickness changed only from 2.6 to 2.1 nm. The corresponding water content in the confined NP layer decreased insignificantly from 28.9 ± 12.8 to 24.7 ± 13.6 vol%.

Since at $D/D_0 = 1.0$, the volume fraction of water, ϕ_w, of 80.8 vol % was close to the water volume fraction of 80.2 vol % for an individual PhG NP (as determined by SANS),[27] we conclude that the confined layer was composed of close-packed PhG NPs, consistent with the AFM results shown in Figure 1e. This concentration also coincides with the onset of sol-gel transition in PhG NP dispersions,[35] suggesting that the uncompressed confined film of the NPs at $D/D_0 = 1.0$ forms a mechanically weak hydrogel. Figure 4c schematically illustrates the mechanism of water expulsion from the confined PhG NP hydrogel layer. We recall that water molecules in hydrogels are categorized in two distinct groups, namely, bound and unbound water molecules.[47] Unbound water molecules in hydrogels have thermodynamic properties similar to those of water molecules in liquid state but they are trapped in the polymer network,[47] whereas bound water molecules are hydrogen-bonded to the polymer chains and thus have different thermodynamic properties than free water molecules. By measuring the enthalpy of fusion of water using differential scanning calorimetry (DSC), we characterized these two populations of water molecules in a PhG NP hydrogel with 19 vol% polymer content, equivalent to the concentration of polymer in the uncompressed confined film. At this concentration, fully hydrated PhG NPs are close-packed, with no interstitial water between them.[35,36] The DSC results indicate that out of 80.8 vol % water existing in the NP film, 55.1±1.5 vol% is in the unbound state, whereas 25.7±1.5 vol% of water is hydrogen-bonded state (Figure S6, Supporting Information). Compressing the film down to D/D0 = 0.4 in the weak-confinement regime did not significantly change the volume fraction of water and polymer in the film. Flattening of

the confined layers of PhG NPs and lateral rearrangements of polymer chains (Figure 4c, i) resulted in squeezing out a fraction of NPs from the contact area. Therefore, in this regime, the volume fractions of the polymer and water remained invariant. Further compression of the confined layer to D/D_0 = 0.08 in the moderate-confinement regime, however, resulted in a decrease in ϕ_w to 28.9 ± 12.8 vol%, which was attributed to the expulsion of unbound water from the NPs layer (Figure 4c, ii). The insignificant decrease in water volume fraction in the strong-confinement regime from 28.9 ± 12.8 to 24.7 ± 13.6 vol% is attributed to a slight expulsion of bound water as shown in Figure 4c, (iii). This measured fraction of bound water from the refractive index analysis is consistent with the 25.7 vol% fraction of bound water molecules measured using DSC.

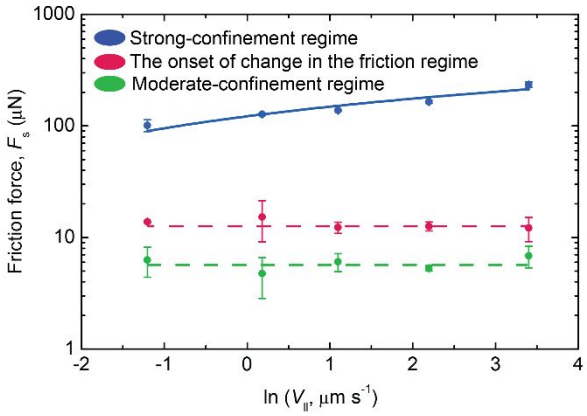

Figure 5. Velocity-dependence of the friction force in the moderate-confinement regime (P = 1.2 MPa), in the onset of change in the lubrication regime (P = 2.4 MPa), and in the strong-confinement regime (P = 5.0 MPa). The dashed lines are for eye guidance. The solid line is the best linear fit, $F_s = A + B.\ln(V_{II})$, indicating an Eyring-like rate activated process.

Confinement-induced dehydration of the PhG NPs significantly affects the mechanism of frictional energy dissipation in the lubricating film. Figure 5 shows that the variation of the friction force with the sliding velocity depends on the lubrication regime. Velocity independent lubrication was observed in the moderate-confinement regime. In the strong-confinement regime, however, the friction force weakly increased with the sliding velocity. We attribute velocity-independent lubrication in the moderate-confinement regime to a "self-regulating" lubrication mechanism that has been previously reported for lubricating polymer brushes.[14,48,49] According to this mechanism, compressed polymer chains adsorbed to the opposing surfaces form an interpenetrating zone with thickness δ. The shear rate in this zone is equivalent to V_{II}/δ, where V_{II} is the sliding velocity. The polymer chains in this zone relax at a rate of $1/\tau(\delta)$, where $\tau(\delta)$ is the δ-dependent relaxation time of the chains, and the friction force between the polymer layers is velocity-independent when $1/\tau(\delta) = V_{II}/\delta$. For this equality to hold, the polymer chain relaxation time and the degree of the interpenetration have to be adjusted in the interpenetrating zone in a self-regulatory manner, which requires rearrangement and mobility of the polymer chains under shear. This mechanism relies on polymer relaxation time $\tau(\delta)$ in the interpenetration region, rather than the entire chain.[49] In the present work, due to the presence of unbound water content in the PhG NP layer in the moderate-confinement regime and fast dynamics (rearrangements) of polymer chains in the interpenetration zone, this self-regulation mechanism remains valid, as evident from the velocity-independent friction force. In addition, branched polymers are expected to exhibit stronger repulsive forces when forced to overlap.[46] Therefore, branched PhG NPs would show a stronger steric repulsion between the polymer chains, thus facilitating the decrease in the thickness of the interpenetration zone at high sliding velocities, which is required for maintaining a constant low fiction coefficient. This mechanism, is exclusive to fluid polymer films and prevails in the low- and moderate-confinement regimes, because of the presence of unbound water molecules in the PhG NP layer at the shearing interface. In the strong-confinement regime, however, closed-pack polymer branches of PhG NPs are only separated by hydrogen-bonded water molecules. The logarithmic dependence of the fric-tion force with the sliding velocity that is observed in this regime is reminiscent of Eyring-like rate-activated process, which has been reported for solid-friction and boundary lubrication systems.[50] According to this mechanism, at high compressive pressures, surface (molecular) asperities have to overcome an energy barrier ΔE, when sliding past each other. This effect gives rise to a friction force that is logarithmically related to the sliding velocity V_{II}, through the relation $F_s = A + B.\ln(V_{II})$, where A and B are constants related to the energy barrier, temperature, contact area and the stress activated volume.[11,51] This rate-activated lubrication mechanism has been reported for hydration lubrication by bound hydration molecules surrounding adsorbed counterions at charged surfaces.[11,51] Therefore, from the velocity dependence of the friction force in the PhG NPs layers, it is inferred that in the strong-confinement regime sliding the bound hydration shells past each other dictates the energy dissipation mechanism, whereas in the moderate confinement regime viscous dissipation due to the fluidity of unbound water molecules and mobility of polymer chains is responsible for the lubrication.

Monitoring the rheological properties of the polymer film at different confinement degrees provides further evidence of different energy dissipation mechanisms depending on the confinement regime. The effective viscosity of the confined NP layer was determined by oscillating the upper surface and measuring the coupling of the oscillation of the upper surface with the lower surface, which is supported on a cantilever spring with spring stiffness K. The oscillations are in the normal direction to the lower surface with an amplitude A_0 and frequency v, causing the lower surface to oscillate with a relative amplitude A. It has been shown that the effective viscosity of the confined media between the two surfaces follows the equation[52]

$$\eta(D) = \frac{KD}{12\pi^2R^2v}\left[\left(\frac{A_0}{A}\right)^2 - \left(1-\frac{f}{K}\right)^2\right]^{0.5}, \qquad (1)$$

where $f = \mathrm{d}F(D)/\mathrm{d}D$ is the gradient of the normal interaction force between the two surfaces and R = 2 cm is the radius of curvature of the surfaces. Figure 6a shows plots of $12\pi^2R^2v/(K[(A0/A)^2-(1-f/K)^2]^{0.5})$ against the separation distance D with PhG NPs dispersed in the media and adsorbed on the surface. The inverse of the slope of the plotted data gives the viscosity. At large separation distances (D >> 33 nm), the data follows a linear variation with D similar to that in pure water (Figure S7, Supporting Information), whereas at D < 33 nm the slope decreases gradually with the separation distance, which indicates that a more viscous media is detected with increased compression. This trend is consistent with previous measurements for adsorbed polymer layers on surfaces.[15,53] Figure 6b shows the corresponding effective viscosity values *vs*. the degree of layer confinement. The viscosity of the media at D

>> 33 nm (D/D_0 >> 1), was η_{eff} = 0.96 ± 0.05 mPa s, which was similar to 0.97 ± 0.04 mPa s measured for pure water (Figure S7, Supporting Information). At D/D_0 < 1, however, the viscosity increased slightly to 1.3 ± 0.1 mPa s because of the presence of swollen adsorbed NPs in the weak-confinement regime. This viscosity remained unchanged until D/D_0 ≈ 0.4, where the film composition did not change with compression. With further compression, in the moderate-confinement regime, the viscosity

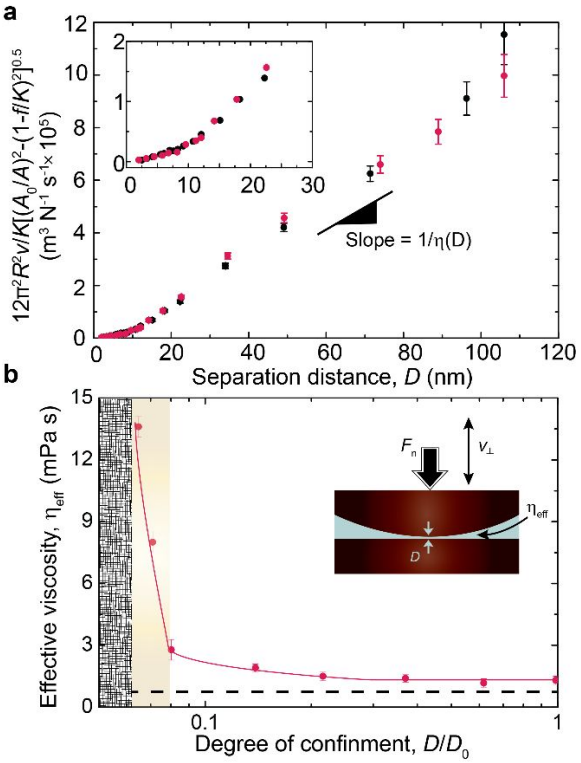

Figure 6. Determination of effective viscosity of the confined PhG NPs film. (a) Plot of viscosity measurements using normal oscillation of surfaces. The viscosity is determined from the inverse of the slope at different separation distances. The inset shows the magnified region at D < 30 nm, where the viscosity increases because of the presence of the NPs layer on the surface. Red and black show two independent measurements. (b) The measured viscosity *vs*. the degree of confinement. The patterned and yellow regions highlight the same confinement limits as in Figure 4. The inset schematically illustrates the viscosity measurement. The dashed line shows the viscosity η_{eff} = 0.96 ± 0.05 mPa s at D/D_0 >> 1. The solid line is given for eye guidance.

increased to 2.8 ± 0.5 mPa s at D/D_0 ≈ 0.08, which is attributed to unbound water exudation and increased polymer fraction in the film. Nevertheless, such low viscosity values still indicate effective viscous dissipation in the film. In addition, in the medium-confinement regime at 0.08< D/D_0 < 0.4, water expulsion contributes to an increase in the bulk modulus of the adsorbed NP film, as suggested by a recent study showing that confinement-induced dehydration of PhG NPs leads to an increase in their bulk modulus.[36] In the strong-confinement regime (0.065 ≤ D/D_0 ≤ 0.080), the effective viscosity sharply increased to 13.6 ± 0.5 mPa s. Considering that the composition of the film does not change significantly in this regime, this increase in viscosity is attributed to the enhanced resistance that the sliding close-packed glucose and water molecules experience during their rearrangements.

The analysis of the extent of hydration and energy dissipation in the confined PhG NP layer suggests that the mechanism of superlubrication originates from different states of water molecules in the NP layer, as illustrated in Scheme 1. Previous reports suggest that confined nanometer-thick film of water exhibit excellent energy dissipation capability that contributes to surface lubrication.[54,55] However, retaining water molecules in a confined layer under high pressures is challenging and requires binding them transiently to the surfaces through various molecular interactions. Water molecules that are bound to hydrophilic moieties *via* hydrogen bonding or electrostatic interactions showed excellent lubrication properties, despite bound water higher viscosity and less efficient energy dissipation compared to unbound water.[11]

In adsorbed PhG NP layers, in addition to bound water molecules, the highly hydrophilic and densely packed hydroxyl groups trap the unbound water molecules in a three-dimensional branched polymer network. Therefore, the unbound water molecules remain in the confined layer under up to 2.4 MPa pressures (in the weak- and moderate confinement regimes, D/D_0 > 0.08) and strongly contribute to the lubrication properties. Although such trapping of unbound water occurs in hydrogels, the

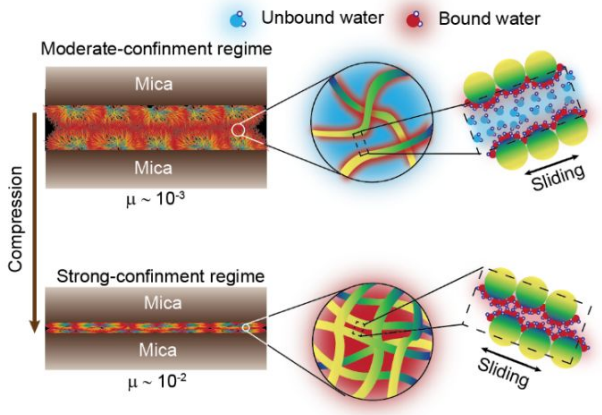

Scheme 1. Illustration of the confined PhG NPs layer in the moderate (top) and strong (bottom) confinement regimes. The zoomed-in areas show polymer and water molecules in the two regimes. This schematic does not show interactions between hydroxyl groups of the PhG NPs and silanol groups of mica.

superlubricating performance of unbound water molecules was not observed in boundary lubricating crosslinked polymer films. Experimental studies have shown that, despite their strong water retention, crosslinked end-grafted polymers result in higher friction coefficient compared to non-crosslinked end-grafted polymers.[56,57] Molecular dynamic simulations have also shown that intermolecular constraints in crosslinked end-grafted brushes in form of hydrogels induce resistance to shear, and negatively affects the lubrication performance.[58] Therefore, the design of superlubricating hydrogels usually involves incorporating non-crosslinked brushes at the hydrogel surface.[59,60] In the case of the adsorbed PhG NP layer, however, no entanglement (physical crosslinking) occurs between the polymer branches in the confined layer even under strong compressions. Therefore, lubrication in this layer benefits from excellent water retention properties of hydrogels, without the negative effects of polymer crosslinking on the energy dissipation.

In the strong-confinement regime (D/D_0 < 0.08, P > 2.4 MPa), however, when only bound water molecules remain in the NP layer, the lubrication is governed by energy dissipation in the

bound hydrtion shells. Energy dissipation in the bound hydration shells causes a significant decrease in the heat generated from irreversible conversion of potential to kinetic energy following the overcoming of the energy barrier as the molecules slide past each other. This effect decreases the friction force by some orders of magnitude compared to non-hydrated molecules.[7] To clarify why the energy disspipation is more efficient with unbound water molecules, we refer to the different dynamics of water molecules in the unbound and bound states. In the unbound state, water reorientation occurs on a time scale of ~ 2 ps, whereas in the bound hydration shells this time scale increases to several tens of picoseconds.[61] An order of magnitude slower dynamics of the water molecules in the bound state compared to unbound state results in weaker energy dissipation in the confined NP layer, as evident from the viscosity and friction force being one order of magnitde larger in the strong-confinment regime than in the moderate-confinment regime.

The friction coefficient of the bound hydration shells in the PhG NP layer in the strong confinement regime, ~10^{-2}, is larger than that for hydration shells of adsorbed ions, ~10^{-4}-10^{-3}, reported for adsorbed Na^+ ions on mica surfaces. This difference can be explained by the higher concentration of bound water molecules in the hydration shells of the Na^+ ions. The number of bound water molecules in the hydration shell of glucose monomers is 2-3 (Table S1), whereas for Na^+ ions this number is 5.[62] Considering that the diameter of glucose monomers in the PhG NPs is 0.7 nm,[27] and Na^+ ions occupy the negatively charged lattice sites on mica surface that are 0.7 nm apart,[11] the concentration of bound water molecules in the hydration shells of a film of adsorbed Na^+ ions on mica surface is approximately twice higher than that in the hydration shell of close-packed glucose monomers at the rubbing interface. In addition, electrostatic interactions can be another factor contributing to the lower friction coefficient of the adsorbed ion layers, compared to our uncharged NP films. However, from the practical point of view, bound hydration shells in PhG NP layers are advantageous lubricating systems, because of their wear resistance properties. In the presence of subnanometric adsorbed bare ion layers, on atomically smooth mica surfaces, the rubbing surfaces were easily damaged, because of misalignment of mica lattices at the rubbing contact area (mica surface roughness).[11] With PhG layers of few nanometer thickness, however, such effects of surface asperities are smeared, and the NP layers act as a wear-protective layer, in addition to reservoirs of bound and unbound water for superlubrication. Another important mechanism that may contribute to the wear-resistant properties of the PhG NP film is the ability of the NPs to "self-heal" their attachment to the surface during shear experiments. These NPs are adsorbed to mica by forming hydrogen bonds between their abundant hydroxyl groups and mica surface silanol group. Hydrogen bonding is reversible and can be broken at high shear rates, however, a highly branched and dense nature of PhG NPs ensures adsorption of another branch to the surface when such bond is broken, thereby self-healing the lubricating film. Therefore, we never observed damage of the rubbing surfaces coated with PhG NP layers with pressures up to 8.1 MPa, as shown in Figure S4.

CONCLUSION

In this study, we introduced highly branched PhG NPs as biosourced boundary superlubricants. The NPs form dense highly hydrated adsorbed layers on mica surfaces, which even at the high degrees of confinement do not exhibit attractive interactions or entanglement. Our results provide evidence of the synergistic contribution of bound and unbound water molecules to superlubrication properties of PhG NP layers. Up to 2.4 MPa normal pressure, confined NP layers retain unbound water molecules, which results in an ultralow friction coefficient of 10^{-3}. At higher normal pressure (up to 8.1 MPa), water molecules hydrogen-bonded to glucose monomers remain in the layer, leading to a friction coefficient of 10^{-2}, owing to hydration lubrication. The lubricating performance of the nature-derived PhG NPs is comparable to the state-of-the-art synthetic polymeric lubricants.[12,14,37] Due to their biocompatibility, PhG NPs are a very promising candidate for lubrication in biological environments. Chemical and physical modification of these NPs would provide the capability of combining their excellent lubricating performance with drug delivery applications.

EXPERIMENTAL SECTION

Materials. PhG NPs were kindly provided by MIREXUS Biotecnologies Inc., following their extraction from sweet corn kernels, purification and subsequent characterization.[27] Aqueous dispersions of PhG NPs were prepared by dispersing them in deionized water (resistivity 18.2 MΩ cm, from the Milli-Q Water Purification System). The dispersion was further purified by dialysis against deionized water using a cellulose acetate membrane (Sigma Aldrich Dialysis Membrane Tubing, with molecular-weight cut-off 12 kDa) for seven days, with water replacement twice a day. The final concentration of the PhG NPs in the dispersion (7.8 mg mL^{-1}) was determined by measuring NPs dry mass. The dispersion was diluted to 20-1000 μg mL^{-1} PhG concentrations prior to the experiments. For the surface force and atomic force imaging experiments, Grade 1 ruby-mica was supplied by S&J Trading. Platinum wire (99.99 %) with diameter 0.25 mm was purchased from Sigma Aldrich Canada.

Surface force measurements

Surface preparation. Back-silvered mica surfaces were prepared following a previously reported protocol.[63,64] Briefly, freshly-cleaved mica sheets with thickness 1-3 μm were cut using a hot platinum wire, and silver-coated by physical vapor deposition (Covap PVD, Angstrom Engineering Inc.) at a deposition rate of 0.2 nm s^{-1} to a final silver thickness of 55 nm. The back-silvered mica pieces were then glued (silver down) to cylindrical glass discs (radius R = 2 cm) for the surface force measurements.

The glass discs carrying the mica sheets were mounted in a cross-cylindrical configuration on the surface force apparatus (SFA 2000 [65]) for determining the reference contact point, which was mica-mica contact in dry air. The SFA chamber was purged with an Argon flow for 30 min to dehumidify the surfaces. The surfaces were approached to each other by a micrometer screw gauge, while white light beam was passing through the surfaces. Fringes of equal chromatic order (FECO) were generated by multiple reflection of the light beam between the two back-silvered mica sheets.[66] At contact, where the surfaces slightly deform, the position of fringes of equal chromatic order (FECO) was recorded using a spectrometer and a CCD camera, and was used as the reference mica-mica contact point in a dry condition.

Normal forces measurements. An aqueous dispersion with PhG NP concentration of 20, 100 or 1000 μg mL^{-1} was injected between the mica surfaces and left unperturbed for one hour. The surfaces were then approached using a DC motor at a constant speed of 3 nm s^{-1} until the immediate contact. At this point the surfaces were compressed for 10 min before they were separated to a final separation distance of ≈ 600 nm, at a constant speed of 6 nm s^{-1}. During the approach and separation, the normal forces were recorded by measuring the deflection of the spring cantilever supporting the lower surface.[43,66–68] For each PhG NP

concentration, three compression-separation cycles were performed on the same contact area, immediately after one another as described above. These three cycles were repeated in at least, three independent experiments.

Friction force measurements. The friction force was measured at different normal loads (or different separation distances). The shear cycles were applied when the PhG NP-coated surfaces came to contact and the surface separation was comparable with the adsorbed NP dimensions. A piezoelectric bimorph drove the lower surface in a back and forth motion at a constant sliding frequency of 50 mHz controlled by a waveform generator (Agilent 33250A, Agilent Technologies, Inc.). The shear force transmitted to the upper surface was detected by semiconductor strain gauges. The separation distance was also continuously recorded during the friction experiments by monitoring the FECO position. Five shearing cycles were applied at each load to ensure the lubrication properties of the PhG NP layer do not change. A total of more than 100 shear cycles were applied to the same contact area in a single experiment. To examine the dependence of friction force on shear frequency, the latter was changed in the range of 5-500 mHz at different fixed normal loads of ≈ 1, 3 and 8 mN. The pressure between the compressed surfaces was calculated as $P = F_n/\pi a^2$, where F_n is the normal load and a is the radius of the deformed area.

Viscosity measurements. The effective viscosity of the liquid confined between mica surfaces was measured using the SFA following a previously reported protocol.[52] For this measurement, the upper mica surface was attached to a piezoelectric crystal, and an alternating current was supplied to the crystal to oscillate the surface at an amplitude of A_0 and frequency of v, normal to the bottom surface. At large surface separation, the lower surface was not affected by the oscillation of the upper surface, and the FECO also oscillated with amplitude A_0. As the surfaces approached each other, the oscillation of the upper surface was transmitted through the confined liquid to the lower surface, which was supported on a cantilever spring with spring constant K. Eventually, when the surfaces were close enough, they oscillated concurrently with the same amplitude, as their motions were coupled. Therefore, the amplitude of the oscillation of the separation distance, A, decreased from A_0 at large separations to close to zero, when the motions of the surfaces were coupled. Equation (1) was used to extract the viscosity as described above. In these experiments the applied AC voltage had an amplitude of 2.5 V, equivalent to $A_0 \approx 11$ nm, and a frequency of 0.5 Hz. The effective viscosity of thin polymer films may differ from bulk rheological properties of the NP dispersions, due to significantly smaller oscillation amplitudes used in our measurements in comparison to those conventionally used in macroscopic rheological experiments.

Refractive index measurements. Analysis of the FECO can be used to estimate the value of refractive index of the confined fluid between the mica surfaces.[65] The refractive index, n, was calculated from[65]

$$n = n_{mica}\sqrt{\frac{(j-1)F_{j-1}}{jF_j}\cdot\frac{\lambda_{j-1}^{D}-\lambda_{j-1}^{0}}{\lambda_j^{D}-\lambda_j^{0}}}, \qquad (2)$$

where $n_{mica} = 1.593 + 4.76 \times 10^5/\lambda_j^{D2}$, is the average refractive index of mica, j is the fringe order, and $F_j \approx 1.024 + 1/j$. Here, λ_j^D is the wavelength position of the j^{th} fringe, with the fluid between the surfaces, and λ_j^0 is the wavelength position of the j^{th} fringe for mica-mica contact in air. The resulting refractive index values have a standard deviation of ±0.001 that gradually increases to ±0.02 as the degree of confinement decreases from D / D_0 = 1.0 to D / D_0 = 0.06. For clarity, the refractive index values and their corresponding volume fractions were also shown by averaging the data and presenting them as discrete data points. Each discrete data point presented by dark-blue symbols represents average and standard deviation of all data points (light blue circles) present in a region of x axis represented by the diameter of the dark-blue circle.

Atomic force microscopy. PhG NP dispersions with concentrations of 0, 20, 100 and 1000 μg mL^{-1} were deposited on freshly cleaved mica sheets and left unperturbed for 1 hour to adsorb. The dispersion was then removed from the surface, and the surface was dried using a strong flow of compressed nitrogen. Atomic force microscopy height images were acquired using a Bruker Inspire™ in tapping mode using a platinum/iridium-coated tip (NanoWorld Arrow-NCPt, force constant = 42 N/m, resonance frequency = 285 kHz, tip radius < 25 nm) in dry air. The data were recorded using the NanoScope v9.40 software package. To account for the effect of tip radius in AFM imaging, we conducted a deconvolution process using Mountains®8 software, with tip radius of 25 nm (measured using scanning electron microscopy (SEM), as shown in Figure S3.

Dynamic light scattering. Size distribution and ζ-potential of the PhG NPs were characterized using a Zetasizer Nano-ZS (Malvern Instruments Ltd.) at a scattering angle of 173º. The dispersion was equilibrated at 294 K for 2 min before each measurement. The reported data show mean and standard deviations of three measurements.

Refractive index of PhG dispersions. The refractive index of the PhG NPs dispersions with concentrations in the range 0-30 wt% were measured using an Abbe refractometer (Reichert Abbe Mark II, Reichert Technologies Inc.) with sodium D line (589.3 nm) illumination at 22 ºC.

Differential scanning calorimetry. The fraction of bound/unbound water in a 29 wt% (equivalent to 19 vol%, dry NP basis) PhG dispersion was determined using a differential scanning calorimeter (Q2000, TA instruments), following a previously reported protocol.[69,70] The PhG NPs hydrogel specimen (12 mg) was placed in the DSC chamber, sealed and cooled to -50 ºC at a rate of 5 ºC min^{-1}, and left for 5 min to equilibrate. The hydrogel was then reheated at 5 ºC min^{-1} to 40 ºC. The melting point of freezing unbound water was observed at ≈ 0 ºC, and the corresponding enthalpy of fusion ΔH_{exp} of 235 J g^{-1}, was used to calculate the fraction of unbound water, X_{UB}, based on water enthalpy of fusion, ΔH_w of 330 J g^{-1} (measured following the same protocol used for the hydrogel), according to $X_{UB} = \Delta H_{exp}/\Delta H_W$.

ASSOCIATED CONTENT

Supporting Information

The supporting information is available including additional experimental details and data obtained using dynamic light scattering, atomic force microscopy, differential scanning calorimetry and the surface forces apparatus.

AUTHOR INFORMATION

Corresponding Authors

eugenia.kumacheva@utoronto.ca;

xavier.banquy@umontreal.ca;

Author Contributions

The manuscript was written through contributions of all authors. All authors have given approval to the final version of the manuscript.

Notes

The authors declare no competing financial interests.

ACKNOWLEDGMENT

The authors thank MIREXUS Biotechnologies Inc. for providing the NPs and helpful discussions. We thank Ning Yan and Nicolas Tanguy for their assistance in conducting DSC measurements, and Ilya Gourevich for his assistance in SEM imaging. V. A. appreciates financial support from Fonds de Recherche du Quebec (FRQ-NT) postdoctoral fellowship program. E. K. and X. B. acknowledge support from NSERC (Discovery) and Canada Research Chair program.

REFERENCES

(1) Adibnia, V.; Mirbagheri, M.; Faivre, J.; Robert, J.; Lee, J.; Matyjaszewski, K.; Lee, D. W.; Banquy, X. Bioinspired Polymers for Lubrication and Wear Resistance. *Prog. Polym. Sci.* **2020**, *110*, 101298.

(2) Cooper, B. G.; Catalina Bordeianu; Nazarian, A.; Snyder, B. D.; Grinstaff, M. W. Active Agents, Biomaterials, and Technologies to Improve Biolubrication and Strengthen Soft Tissues. *Biomaterials* **2018**, *181*, 210–226.

(3) Schwarz, I. M.; Hills, B. A. Surface-Active Phospholipid as the Lubricating Component of Lubricin. *Br. J. Rheumatol.* **1998**, *37*, 21–26.

(4) Seror, J.; Zhu, L.; Goldberg, R.; Day, A. J.; Klein, J. Supramolecular Synergy in the Boundary Lubrication of Synovial Joints. *Nat. Commun.* **2015**, *6*, 6497.

(5) Raj, A.; Wang, M.; Zander, T.; Wieland, D. C. F.; Liu, X.; An, J.; Garamus, V. M.; Willumeit-Römer, R.; Fielden, M.; Claesson, P. M.; Dėdinaitė, A. Lubrication Synergy: Mixture of Hyaluronan and Dipalmitoylphosphatidylcholine (DPPC) Vesicles. *J. Colloid Interface Sci.* **2017**, *488*, 225–233.

(6) Jahn, S.; Seror, J.; Klein, J. Lubrication of Articular Cartilage. *Annu. Rev. Biomed. Eng.* **2016**, *18*, 235–258.

(7) Adibnia, V.; Mirbagheri, M.; Salimi, S.; De Crescenzo, G.; Banquy, X. Nonspecific Interactions in Biomedical Applications. *Curr. Opin. Colloid Interface Sci.* **2020**, *47*, 70–83.

(8) Wang, Y.; Sun, Y.; Gu, Y.; Zhang, H. Articular Cartilage-Inspired Surface Functionalization for Enhanced Lubrication. *Adv. Mater. Interfaces* **2019**, *6*, 1–7.

(9) Jahn, S.; Klein, J. Hydration Lubrication: The Macromolecular Domain. *Macromolecules* **2015**, *48*, 5059–5075.

(10) Li, J.; Cao, W.; Wang, Z.; Ma, M.; Luo, J. Origin of Hydration Lubrication of Zwitterions on Graphene. *Nanoscale* **2018**, *10*, 16887–16894.

(11) Ma, L.; Gaisinskaya-Kipnis, A.; Kampf, N.; Klein, J. Origins of Hydration Lubrication. *Nat. Commun.* **2015**, *6*, 8–13.

(12) Raviv, U.; Giasson, S.; Kampf, N.; Gohy, J. F.; Jérôme, R.; Klein, J. Lubrication by Charged Polymers. *Nature* **2003**, *425*, 163–165.

(13) Yu, J.; Jackson, N. E.; Xu, X.; Morgenstern, Y.; Kaufman, Y.; Ruths, M.; de Pablo, J. J.; Tirrell, M. Multivalent Counterions Diminish the Lubricity of Polyelectrolyte Brushes. *Science.* **2018**, *360*, 1434–1438.

(14) Chen, M.; Briscoe, W. H.; Armes, S. P.; Klein, J. Lubrication at Physiological Pressures by Polyzwitterionic Brushes. *Science.* **2009**, *323*, 1698–1701.

(15) Adibnia, V.; Olszewski, M.; De Crescenzo, G.; Matyjaszewski, K.; Banquy, X. Superlubricity of Zwitterionic Bottlebrush Polymers in the Presence of Multivalent Ions. *J. Am. Chem. Soc.* **2020**, *142*, 14843–14847.

(16) Perrino, C.; Lee, S.; Spencer, N. D. End-Grafted Sugar Chains as Aqueous Lubricant Additives: Synthesis and Macrotribological Tests of Poly(l-Lysine)-Graft-Dextran (PLL-g-Dex) Copolymers. *Tribol. Lett.* **2009**, *33*, 83–96.

(17) Liu, P.; Liu, Y.; Yang, Y.; Chen, Z.; Li, J.; Luo, J. Mechanism of Biological Liquid Superlubricity of Brasenia Schreberi Mucilage. *Langmuir* **2014**, *30*, 3811–3816.

(18) Liu, G.; Liu, Z.; Li, N.; Wang, X.; Zhou, F.; Liu, W. Hairy Polyelectrolyte Brushes-Grafted Thermosensitive Microgels as Artificial Synovial Fluid for Simultaneous Biomimetic Lubrication and Arthritis Treatment. *ACS Appl. Mater. Interfaces* **2014**, *6*, 20452–20463.

(19) Liu, G.; Cai, M.; Zhou, F.; Liu, W. Charged Polymer Brushes-Grafted Hollow Silica Nanoparticles as a Novel Promising Material for Simultaneous Joint Lubrication and Treatment. *J. Phys. Chem. B* **2014**, *118*, 4920–4931.

(20) Yang, J.; Han, Y.; Lin, J.; Zhu, Y.; Wang, F.; Deng, L.; Zhang, H.; Xu, X.; Cui, W. Ball-Bearing-Inspired Polyampholyte-Modified Microspheres as Bio-Lubricants Attenuate Osteoarthritis. *Small* **2020**, *2004519*, 1–14.

(21) Lee, H.; Lee, M. Y.; Bhang, S. H.; Kim, B. S.; Kim, Y. S.; Ju, J. H.; Kim, K. S.; Hahn, S. K. Hyaluronate-Gold Nanoparticle/Tocilizumab Complex for the Treatment of Rheumatoid Arthritis. *ACS Nano* **2014**, *8*, 4790–4798.

(22) St.dennis, J. E.; Jin, K.; John, V. T.; Pesika, N. S. Carbon Microspheres as Ball Bearings in Aqueous-Based Lubrication. *ACS Appl. Mater. Interfaces* **2011**, *3*, 2215–2218.

(23) Andablo-Reyes, E.; Yerani, D.; Fu, M.; Liamas, E.; Connell, S.; Torres, O.; Sarkar, A. Microgels as Viscosity Modifiers Influence Lubrication Performance of Continuum. *Soft Matter* **2019**, *15*, 9614–9624.

(24) Anilkumar, P.; Lawson, T. B.; Abbina, S.; Mäkelä, J. T. A.; Sabatelle, R. C.; Takeuchi, L. E.; Snyder, B. D.; Grinstaff, M. W.; Kizhakkedathu, J. N. Mega Macromolecules as Single Molecule Lubricants for Hard and Soft Surfaces. *Nat. Commun.* **2020**, *11*, 2139.

(25) Huang, L.; Yao, Y. Particulate Structure of Phytoglycogen Nanoparticles Probed Using Amyloglucosidase. *Carbohydr. Polym.* **2011**, *83*, 1665–1671.

(26) Besford, Q. A.; Cavalieri, F.; Caruso, F. Glycogen as a Building Block for Advanced Biological Materials. *Adv. Mater.* **2020**, *32*, 1–23.

(27) Nickels, J. D.; Atkinson, J.; Papp-Szabo, E.; Stanley, C.;

Diallo, S. O.; Perticaroli, S.; Baylis, B.; Mahon, P.; Ehlers, G.; Katsaras, J.; Dutcher, J. R. Structure and Hydration of Highly-Branched, Monodisperse Phytoglycogen Nanoparticles. *Biomacromolecules* **2016**, *17*, 735–743.

(28) Meléndez, R.; Meléndez-Hevia, E.; Cascante, M. How Did Glycogen Structure Evolve to Satisfy the Requirement for Rapid Mobilization of Glucose? A Problem of Physical Constraints in Structure Building. *J. Mol. Evol.* **1997**, *45*, 446–455.

(29) Grossutti, M.; Dutcher, J. R. Correlation between Chain Architecture and Hydration Water Structure in Polysaccharides. *Biomacromolecules* **2016**, *17*, 1198–1204.

(30) Perticaroli, S.; Nakanishi, M.; Pashkovski, E.; Sokolov, A. P. Dynamics of Hydration Water in Sugars and Peptides Solutions. *J. Phys. Chem. B* **2013**, *117*, 7729–7736.

(31) Lupi, L.; Comez, L.; Paolantoni, M.; Perticaroli, S.; Sassi, P.; Morresi, A.; Ladanyi, B. M.; Fioretto, D. Hydration and Aggregation in Mono- and Disaccharide Aqueous Solutions by Gigahertz-to-Terahertz Light Scattering and Molecular Dynamics Simulations. *J. Phys. Chem. B* **2012**, *116*, 14760–14767.

(32) Arai, K.; Shikata, T. Hydration/Dehydration Behavior of Cellulose Ethers in Aqueous Solution. *Macromolecules* **2017**, *50*, 5920–5928.

(33) Du, C.; Mendelson, A. A.; Guan, Q.; Chapanian, R.; Chafeeva, I.; da Roza, G.; Kizhakkedathu, J. N. The Size-Dependent Efficacy and Biocompatibility of Hyperbranched Polyglycerol in Peritoneal Dialysis. *Biomaterials* **2014**, *35*, 1378–1389.

(34) Simmons, J.; Nickels, J. D.; Michalski, M.; Grossutti, M.; Shamana, H.; Stanley, C. B.; Schwan, A. L.; Katsaras, J.; Dutcher, J. R. Structure, Hydration, and Interactions of Native and Hydrophobically Modified Phytoglycogen Nanoparticles. *Biomacromolecules* **2020**, *21*, 4053–4062.

(35) Shamana, H.; Grossutti, M.; Papp-Szabo, E.; Miki, C.; Dutcher, J. R. Unusual Polysaccharide Rheology of Aqueous Dispersions of Soft Phytoglycogen Nanoparticles. *Soft Matter* **2018**, *14*, 6496–6505.

(36) Grossutti, M.; Dutcher, J. R. Correlation of Mechanical and Hydration Properties of Soft Phytoglycogen Nanoparticles. *Carbohydr. Polym.* **2021**, *251*, 116980.

(37) Lin, W.; Kampf, N.; Klein, J. Designer Nanoparticles as Robust Superlubrication Vectors. *ACS Nano* **2020**, *14*, 7008–7017.

(38) Faivre, J.; Shrestha, B. R.; Xie, G.; Olszewski, M.; Adibnia, V.; Moldovan, F.; Montembault, A.; Sudre, G.; Delair, T.; David, L.; Matyjaszewski, K.; Banquy, X. Intermolecular Interactions between Bottlebrush Polymers Boost the Protection of Surfaces against Frictional Wear. *Chem. Mater.* **2018**, *30*, 4140–4149.

(39) Liu, R.; Boehlein, S. K.; Tracy, W. F.; Resende, M. F. R.; Hudalla, G. A. Characterizing the Physical Properties and Cell Compatibility of Phytoglycogen Extracted from Different Sweet Corn Varieties. *Molecules* **2020**, *25*, 1–15.

(40) Xie, Y.; Yao, Y. Octenylsuccinate Hydroxypropyl Phytoglycogen, a Dendrimer-Like Biopolymer, Solubilizes Poorly Water-Soluble Active Pharmaceutical Ingredients. *Carbohydr. Polym.* **2018**, *180*, 29–37.

(41) Lu, F.; Mencia, A.; Bi, L.; Taylor, A.; Yao, Y.; HogenEsch, H. Dendrimer-Like Alpha-d-Glucan Nanoparticles Activate Dendritic Cells and Are Effective Vaccine Adjuvants. *J. Control. Release* **2015**, *204*, 51–59.

(42) Christenson, H. K.; Thomson, N. H. The Nature of the Air-Cleaved Mica Surface. *Surf. Sci. Rep.* **2016**, *71*, 367–390.

(43) Israelachvili, J. N.; Adams, G. E. Measurement of Forces between Two Mica Surfaces in Aqueous Electrolyte Solutions in the Range 0-100 Nm. *J. Chem. Soc. Faraday Trans. 1 Phys. Chem. Condens. Phases* **1978**, *74*, 975–1001.

(44) Banquy, X.; Le Dévédec, F.; Cheng, H. W.; Faivre, J.; Zhu, J. X. X.; Valtiner, M. Interaction Forces between Pegylated Star-Shaped Polymers at Mica Surfaces. *ACS Appl. Mater. Interfaces* **2017**, *9*, 28027–28033.

(45) Leermakers, F. A. M.; Zhulina, E. B.; Borisov, O. V. Interaction Forces and Lubrication of Dendronized Surfaces. *Curr. Opin. Colloid Interface Sci.* **2017**, *27*, 50–56.

(46) Borisov, O. V.; Zhulina, E. B.; Polotsky, A. A.; Leermakers, F. A. M.; Birshtein, T. M. Interactions between Brushes of Root-Tethered Dendrons. *Macromolecules* **2014**, *47*, 6932–6945.

(47) Gun'ko, V.; Savina, I.; Mikhalovsky, S. Properties of Water Bound in Hydrogels. *Gels* **2017**, *3*, 37.

(48) Schorr, P. A.; Kwan, T. C. B.; Kilbey, S. M.; Shaqfeh, E. S. G.; Tirrell, M. Shear Forces between Tethered Polymer Chains as a Function of Compression, Sliding Velocity, and Solvent Quality. *Macromolecules* **2003**, *36*, 389–398.

(49) Tadmor, R.; Janik, J.; Klein, J.; Fetters, L. J. Sliding Friction with Polymer Brushes. *Phys. Rev. Lett.* **2003**, *91*, 2–5.

(50) Gnecco, E.; Bennewitz, R.; Gyalog, T.; Loppacher, C.; Bammerlin, M.; Meyer, E.; Güntherodt, H. J. Velocity Dependence of Atomic Friction. *Phys. Rev. Lett.* **2000**, *84*, 1172–1175.

(51) Rosenhek-Goldian, I.; Kampf, N.; Klein, J. Trapped Aqueous Films Lubricate Highly Hydrophobic Surfaces. *ACS Nano* **2018**, *12*, 10075−10083.

(52) Israelachvili, J. N. Measurement of the Viscosity of Liquids in Very Thin Films. *J. Colloid Interface Sci.* **1986**, *110*, 263–271.

(53) Lee, D. W.; Banquy, X.; Kristiansen, K.; Kaufman, Y.; Boggs, J. M.; Israelachvili, J. N. Lipid Domains Control Myelin Basic Protein Adsorption and Membrane Interactions between Model Myelin Lipid Bilayers. *Proc. Natl. Acad. Sci. U. S. A.* **2014**, *111*, E768–E775.

(54) Raviv, U.; Laurat, P.; Klein, J. Fluidity of Water Confined to Subnanometre Films. *Nature* **2001**, *413*, 51–54.

(55) Zhu, Y.; Granick, S. Viscosity of Interfacial Water. *Phys. Rev. Lett.* **2001**, *87*, 1–4.

(56) Dehghani, E. S.; Ramakrishna, S. N.; Spencer, N. D.; Benetti, E. M. Controlled Crosslinking Is a Tool To Precisely Modulate the Nanomechanical and Nanotribological Properties of Polymer Brushes. *Macromolecules* **2017**, *50*, 2932–2941.

(57) Li, A.; Ramakrishna, S. N.; Nalam, P. C.; Benetti, E. M.;

Spencer, N. D. Stratified Polymer Grafts: Synthesis and Characterization of Layered "Brush" and "Gel" Structures. *Adv. Mater. Interfaces* **2014**, *1* (1), 1–8.

(58) Singh, M. K.; Ilg, P.; Espinosa-Marzal, R. M.; Kröger, M.; Spencer, N. D. Effect of Crosslinking on the Microtribological Behavior of Model Polymer Brushes. *Tribol. Lett.* **2016**, *63*, 17.

(59) Kaneko, D.; Tada, T.; Kurokawa, T.; Gong, J. P.; Osada, Y. Mechanically Strong Hydrogels with Ultra-Low Frictional Coefficients. *Adv. Mater.* **2005**, *17*, 535–538.

(60) Gong, J. P. Friction and Lubrication of Hydrogels - Its Richness and Complexity. *Soft Matter* **2006**, *2*, 544–552.

(61) Laage, D.; Elsaesser, T.; Hynes, J. T. Water Dynamics in the Hydration Shells of Biomolecules. *Chem. Rev.* **2017**, *117*, 10694–10725.

(62) Rempe, S. B.; Pratt, L. R. The Hydration Number of Na+ in Liquid Water. *Fluid Phase Equilib.* **2001**, *183–184*, 121–132.

(63) Israelachvili, J. N.; Alcantar, N. A.; Maeda, N.; Mates, T. E.; Ruths, M. Preparing Contamination-Free Mica Substrates for Surface Characterization, Force Measurements, and Imaging. *Langmuir* **2004**, *20*, 3616–3622.

(64) Adibnia, V.; Mirbagheri, M.; Latreille, P. L.; De Crescenzo, G.; Rochefort, D.; Banquy, X. Interfacial Forces across Ionic Liquid Solutions: Effects of Ion Concentration and Water Domains. *Langmuir* **2019**, *35*, 15585–15591.

(65) Israelachvili, J.; Min, Y.; Akbulut, M.; Alig, A.; Carver, G.; Greene, W.; Kristiansen, K.; Meyer, E.; Pesika, N.; Rosenberg, K.; Zeng, H. Recent Advances in the Surface Forces Apparatus (SFA) Technique. *Reports Prog. Phys.* **2010**, *73*, 036601.

(66) Israelachvili, J. N. Thin Film Studies Using Multiple-Beam Interferometry. *J. Colloid Interface Sci.* **1973**, *44*, 259–272.

(67) Israelachvili, J.; Min, Y.; Akbulut, M.; Alig, A.; Carver, G.; Greene, W.; Kristiansen, K.; Meyer, E.; Pesika, N.; Rosenberg, K.; Zeng, H. Recent Advances in the Surface Forces Apparatus (SFA) Technique. *Reports Prog. Phys.* **2010**, *73*, 036601.

(68) Pashley, R. M.; Israelachvili, J. N. Dlvo and Hydration Forces between Mica Surfaces in Mg2+, Ca2+, Sr2+, and Ba2+ Chloride Solutions. *J. Colloid Interface Sci.* **1984**, *97*, 446–455.

(69) Cursaru, B.; Stănescu, P. O.; Teodorescu, M. The States of Water in Hydrogels Synthesized from Diepoxy-Terminated Poly(ethylene Glycol)s and Aliphatic Polyamines. *UPB Sci. Bull. Ser. B Chem. Mater. Sci.* **2010**, *72*, 99–114.

(70) Khare, A. R.; Peppas, N. A. Investigation of Hydrogel Water in Polyelectrolyte Gels Using Differential Scanning Calorimetry. *Polymer* **1993**, *34*, 4736–4739.

Table of Contents artwork